Nearly Unattenuated Charge Density Wave Transport in a Linear Chain Conductor Fabricated by Spark Discharge

Peter Arendt

Fritz-Haber-Institute of the Max-Planck-Society, Berlin, Germany

Reprint requests to P. A.; Parkallee 6, 15517 Fürstenwalde, Germany,
E-mail: wasle@fhi-berlin.mpg.de

Z. Naturforsch. **67a,** 29 – 38 (2012) / DOI: 10.5560/ZNA.2011-0054
Received March 30, 2011/ revised August 29, 2011

Chemical preparation techniques have proved in the past unsuitable for the synthesis of linear chain conductors which are said to exhibit anomalously large electrical conductivities via moving charge density waves (CDWs) which are depinned from the underlying linear ionic lattice and move in a direct current (DC) electric field nearly unattenuated. We present a novel technique which uses only purely physical processes to fabricate linear chain conductors which seem to meet all claims laid by the CDW mechanism of conductivity in its ideal form. A spark engraves in an originally low-conducting nonlinear silver-based material, driven far from equilibrium beyond some critical power input, a discharge pattern, inside the branches of which chains of Ag^+-ions run which form a high-conducting current path, along which CDWs may propagate nearly unattenuated. The material obtained exhibits an electrical conductivity which is by four orders of magnitude higher than the conductivity of metallic silver. A simple model is presented to explain this high conductivity and some related phenomena associated with electrical conduction via a moving CDW.

Key words: Linear Chain Conductor; Charge Density Wave Transport; Nonlinear System far from Equilibrium; Filamentary Spark Discharge Pattern.

1. Introduction

The design and synthesis of linear chain conductors which exhibit quasi-one-dimensional metallic behaviour have been the subject of intense experimental investigations over more than four decades. In the (organic and inorganic) linear chain compounds charge density waves (CDWs), periodic distortions of the conduction electron density, accompanied by distortions of the underlying linear ionic lattice, may occur. Below a threshold direct current (DC) electric field E_T the CDWs do not move because they are pinned to the lattice by defects and impurities. The CDWs, however, may break free with the application of small applied fields $E > E_T$. The depinned CDWs then start to contribute to the conductivity. However, anomalously large conductivities do not occur for the compounds in their present state of crystalline perfection despite the intense research work undertaken to use chemical preparation techniques more effectively in synthesizing better chain-like compounds. (For a review on CDWs, see [1].)

The novel technique presented here, which uses only purely physical processes to fabricate linear chain conductors, makes the most of the fact that the emergence of an ordered filamentary structure can arise in a previously unstructured medium (a colloidal silver solution), which has been made nonlinear and then is driven far from equilibrium beyond a certain threshold of electric power input [2].

2. Sample Preparation

The preparation of this new linear conductor proceeds in three steps (for details see [3]).

In the first step, a high alternating current (AC) voltage discharge is passed through a colloidal aqueous silver solution, deposited on a single-layer sheet of glass fibres of 20 μm thickness (6 mm in width and of 5 cm length, equal to the interelectrode distance) mounted on a glass plate, the glass fibres oriented in the direction of current. The discharge is sufficiently energetic to partially disrupt the colloidal silver and render the colloidal silver solution conductive.

In the second step, the conducting state that has hitherto prevailed, exhibiting a nonlinear current–voltage characteristic, is made unstable by passing a DC current through the solution beyond some critical power input: beyond instability the system jumps to a new regime, in which the current is increased within some seconds to some amperes at nearly constant voltage (see Fig. 1 of [3]).

In the third step, a DC voltage is suddenly applied to the sample by contacting a lead-accumulator battery. Along the primary pattern created beyond instability a spark then engraves the final filamentary discharge pattern. A large DC voltage (36 V) is crucial for the evolution of a spark producing a discharge pattern filamentary in nature, as may be concluded from the analogous situation met with the electrodeposition of metal atoms onto the cathode from an ionic solution: electrodeposit patterns exhibit a branched tree-like structure at lower deposition voltages; at higher voltages the deposits become more dense, forming a bunch of rectilinear, parallel filaments with little branching [4].

If the current electrodes are placed on the sample far away (5 cm) from each other, the spark may run from the cathode to the anode as well as in the opposite direction. If cathode and anode have been placed only some millimetres apart from each other with the cathode on the left and the anode on the right, both placed at the left (right) end of the sample, the spark runs from the cathode (anode), passing the anode (cathode), into the zero-electric field region behind the anode (cathode). In each case the spark usually propagates across a distance of about 3 cm (sometimes across the total sample length of 5 cm). During the passage of the spark, which takes about 3 s, a current of about 1 A flows. After the passage of the spark the sample may be cut off from the supporting glass plate and pasted on a piece of cardboard.

In the Figures 1a and 1b the spark has run from the cathode on the left to the anode on the right. A thin white track appears either near the upper (as in Figure 1a) or lower boundary of the sample (as in Figure 1b). The high-conducting current path, which we shall localize in Section 3, does not coincide with the white track, but runs somewhat sideward of it, closer to the boundary of the sample. In any case the high-conducting current path is bounded towards the interior of the sample as well as towards the upper and lower boundary of the sample, respectively, by some matrix which, not affected by the spark, remains low-conducting, short-circuited by the high-conducting path.

Fig. 1. Thin white track appearing near (a) the upper and (b) the lower boundary of the sample, after the spark has run from the cathode (on the left) to the anode (on the right). The length of the samples of 5 cm gives the scale of the photo.

3. Potential Distribution

The spark generates a discharge pattern with rectilinear, closely packed branches (see Section 5) which form the high-conducting current path. When the spark runs from the anode towards the cathode, electrons, attracted towards the anode, leave behind non-compensated Ag^+-ions at the heads of the branches, and a quasi-neutral plasma of ions and electrons behind the positive heads. When the spark runs in the opposite direction, electrons, attracted towards the anode, leave behind excess electrons at the heads of the branches, and a plasma of ions and electrons behind the negative heads (for illustration, see Figs. 12.5 and 12.6 of [5, pp. 335, 338]).

The potential distribution along the sample between cathode and anode is recorded by a standard DC four-probe method by applying the potential probes of a multimeter to the sample (using a Hewlett Packard digital multimeter 3478A with a resolution of 1 μV in the 300 mV measuring range).

Let us draw a DC current of $I = 1$ A through the sample, flowing nearly exclusively through the high-conducting current path, 3 cm in length, embedded in the adjacent low-conducting matrix which becomes short-circuited. In case that the spark has run from the anode to the cathode, the potential (i.e. the potential difference V_x of a potential probe against the cathode at locations x along the current path) steeply rises across a double layer near the cathode nearly to the total voltage applied between cathode and anode of (for illustration, see Figure 2),

$$V_0 \cong 140\,\text{mV}. \tag{1}$$

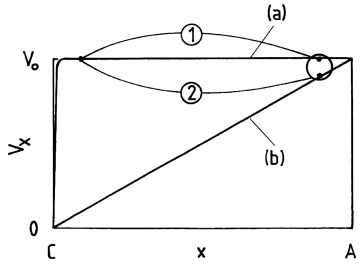

Fig. 2. Potential distribution (a) along the high-conducting current path and (b) along the adjacent low-conducting matrix, with a current flowing through the sample between cathode C and anode A and the potential probes placed as indicated, when the voltage V_h is very small.

In case that the spark has run in the opposite direction, the potential steeply rises across a double layer near the anode in the same way nearly to the total voltage V_0 applied.

In the former case, the double layer consists of non-compensated Ag^+-ions at the heads of the branches, facing a negative surface charge on the copper cathode, the electrons being ejected from the cathode into the double layer under the applied voltage V_0. In the latter case, the double layer consists of excess electrons at the heads of the branches, facing a surface charge of opposite sign on the copper anode, the electrons being ejected from the bulk-near side of the double layer towards the anode under the applied voltage V_0. By taking the potential difference V_0 across the double layer to be about 0.1 V (see (1)) and the distance d between the layers of charges in the double layer to be about 1 nm [6], the electric field strengths V_0/d in the double layer are high enough for an electron to tunnel through the layer and take up the energy eV_0.

The total resistance across the high-conducting current path between cathode and anode, nearly exclusively determined by the resistance across the double layer near the cathode and anode, respectively, and hence nearly independent of the length of the path, becomes

$$R = V_0/I \cong 0.140\,\Omega = \text{const.} \tag{2}$$

This resistance remains constant (i.e. the voltage V_0 is linearly related to the current I) up to currents of 3 – 5 A.

Across the high-conducting current path inside the bulk, i.e. the current path excluding the double layer near the cathode and anode, respectively, the potential rises by only a very small voltage V_h, whose magnitude is independent of the direction along which the spark has run before. On drawing a DC current of $I = 1$ A through the sample, the voltages V_h have, on average, been found to be

$$V_h \cong 0.0003\ \text{mV} \tag{3}$$

taken across a length of

$$l \leq 3.0\ \text{cm} \tag{4}$$

along the current path. V_h is the voltage drop across the plasma of ions and electrons inside the bulk.

The very small (positive) voltage V_h in (3) corresponds to the situation described schematically in Figure 2, Signal (1), in case that the double layer appears near the cathode. It may happen, however, that the signals fluctuate between very small positive and negative values when the tip of the potential probe near the anode alternately touches the high-conducting current path and the low-conducting matrix, as illustrated in Figure 2, Signal (1) and (2). This effect does not occur when the voltage V_h is larger, as illustrated in Figure 3, Signal (3); when in this case the potential probe near the anode touches the low-conducting matrix, the signals remain positive, as illustrated in Figure 3, Signal (4).

The potential difference V_x of a potential probe not placed upon the high-conducting current path but upon the adjacent low-conducting matrix below or above the current path, taken against the cathode at locations x along the matrix, is a linear function of the distance x from the cathode, as is expected for a normal conductor. In [3], we have abraded the high-conducting current path and then measured the Ohmic resistance across the matrix left, 3 cm in length, to be about 100 Ω. That is, the high-conducting current path nearly exclusively carries the total current I, so that we can write for the resistance across the high-conducting cur-

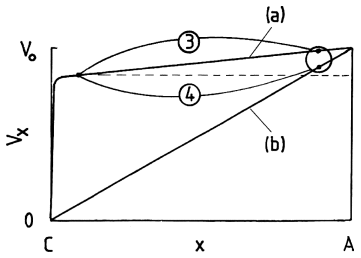

Fig. 3. As in Figure 2, when the voltage V_h is larger.

rent path inside the bulk, ≤ 3 cm in length,

$$R_h = V_h/I \cong 3.0 \cdot 10^{-7}\ \Omega = \text{const.}, \qquad (5)$$

the voltage V_h being linearly related to the current I up to currents of 3 – 5 A.

Despite the potential rise across the double layer near the cathode and anode, respectively, the sample attains the same temperature near both the cathode and the anode, which shows that the electrons tunnel through the double layer near the cathode and anode, respectively, without any energy losses, taking up the energy eV_0. The temperature distribution along the high-conducting current path and low-conducting matrix, respectively, is symmetric about the midpoint, where the temperatures attain their maximum, the high-conducting current path growing warm much less than the low-conducting matrix.

We note that the sum of the potential rises between cathode and anode (i.e., the potential rise across the double layer near cathode and anode, respectively, plus the potential rise V_h across the bulk) proves equal to the total voltage V_0 applied. Also does the current path behave as an Ohmic conductor. This demonstrates that the potential probes do not come to lie upon branches of the discharge pattern which end anywhere and do not connect cathode and anode. Nor do the potential probes grasp beside the branches. This is all the more true since the branches are closely packed (see Section 5), forming a current path which can be considered a 'wire'.

4. Cross-Sectional Area of the High-Conducting Current Path

The width of the high-conducting current path is determined as illustrated in Figure 4: one potential probe of the multimeter is put down to the high-conducting current path near the anode, while the other potential probe is moved across the sample perpendicular to the current path near the cathode, the forward shift of the potential probe controlled with the help of an external micrometer: as long as the mobile potential probe contacts the low-conducting matrix below or above the current path, the potential difference V of the mobile potential probe against the fixed potential probe is about 90 mV across distances between the two potential probes of 2 cm at a current of 1 A flowing through the sample. As soon as, however, the mobile potential

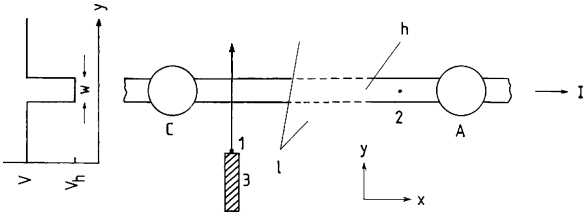

Fig. 4. Potential differences V and V_h of a mobile potential probe against a fixed potential probe at locations y perpendicular to the current path, when in the x-direction a current I flows through the sample. The notation is 1, mobile potential probe; 2, fixed potential probe; 3, micrometer head; C, cathode; A, anode; h, high-conducting current path; l, low-conducting matrix; and w, width of high-conducting current path.

probe contacts the high-conducting current path, the potential steeply drops to the voltage V_h (see Figure 5).

We find that the width of the high-conducting current path, on average, is

$$w \cong 0.040\ \text{cm}.$$

The thickness of the high-conducting current path is determined with an external micrometer as the difference between (i) the thickness of the glass plate (upon which the sample has been prepared as its support) plus

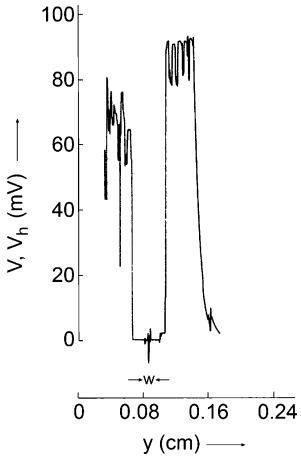

Fig. 5. Potential differences V and V_h of a mobile potential probe against a fixed potential probe. The mobile potential probe is moved from some origin $y = 0$, positioned on the low-conducting matrix below the high-conducting current path, towards the upper boundary of the sample, passing with increasing y across the high-conducting current path of width w. The distance between the two potential probes in the direction of current flow is 2 cm; the current I flowing through the sample is 1 A.

the thickness of the sample at places where the current path runs and (ii) the thickness of the glass plate alone. We obtain

$$t \cong 0.015\,\text{cm},$$

which is large compared to the thickness (20 µm) of the single-layer sheet of glass fibres, whose space requirement is neglected in the following. Hence, the cross-sectional area of the high-conducting current path amounts to

$$wt \cong 6.0 \cdot 10^{-4}\,\text{cm}^2. \quad (6)$$

5. Scanning Electron Microscope Studies

Scanning electron microscopy (SEM) is used to look at the structure of small sample areas. Figure 6a shows the high-conducting current path on the whole, bounded by the adjacent low-conducting interior of the sample (bottom) and the adjacent low-conducting upper boundary of the sample (top). The apparent width w of the high-conducting current path in this figure is about 600 µm for this sample.

Figures 6b – 6d show the microstructure with increasing magnification. In Figure 6b (bottom) two par-

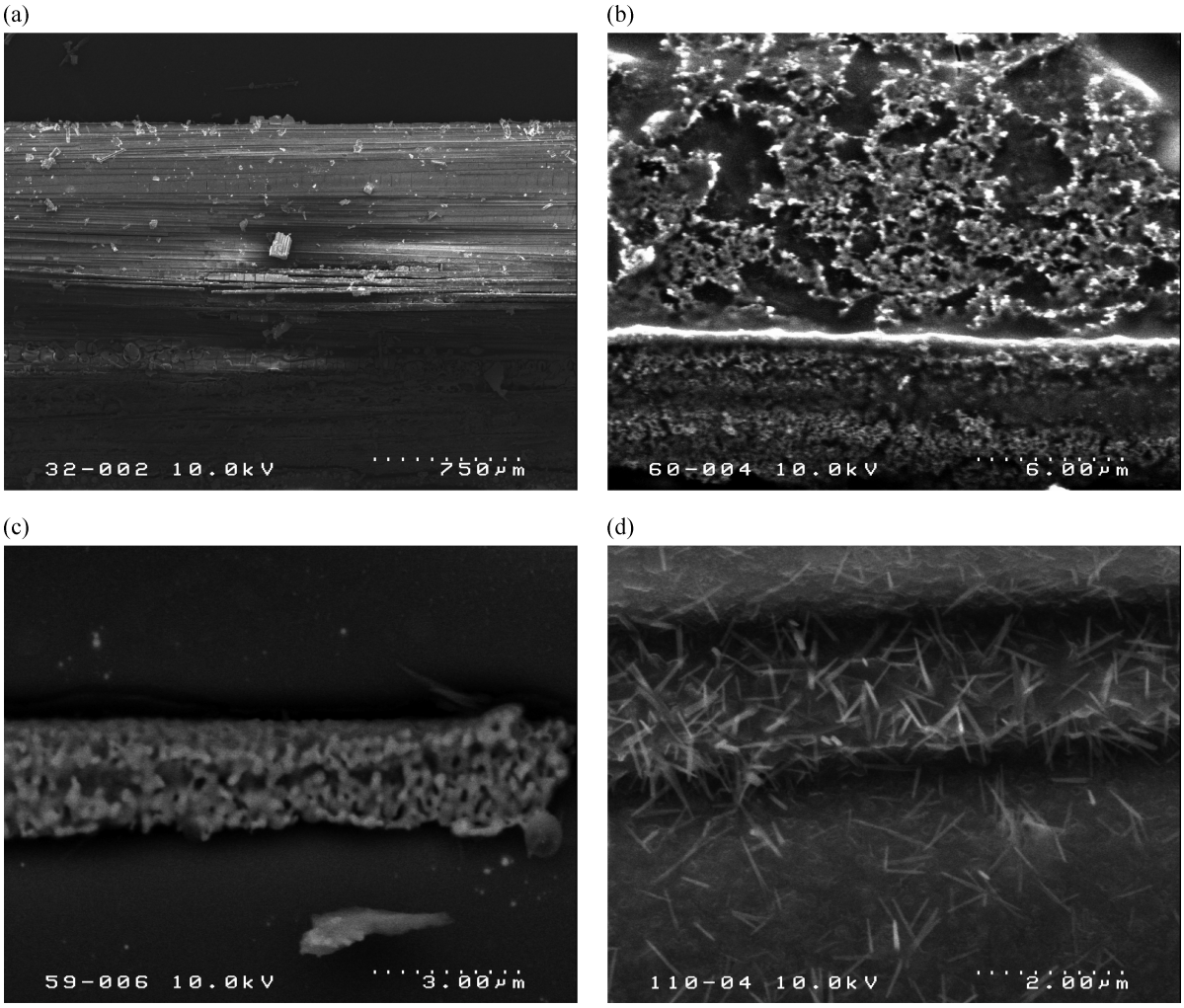

Fig. 6. SEM images (recorded at 10 kV) of a high-conducting sample area, taken in the secondary electron-mode with increasing magnification. (a) High-conducting path of 600 µm width. (b) Two high-conducting filaments visible below the white track. (c) Detailed view of one high-conducting filament. (d) Three closely packed high-conducting filaments.

allel, closely packed filaments aligned along the electric field have grown, bounded towards the interior of the sample (top) by an open structure, out of which none such filaments have organized and which belongs to the low-conducting matrix, not affected by the spark. The high-conducting filaments run somewhat sideward of the white track, closer to the lower boundary of the sample (bottom). In Figure 6c one filament, in Figure 6d a bunch of three parallel, closely packed filaments is seen. All filaments have a diameter of 1.5 – 2.0 µm. Because this diameter is comparable with that calculated below (see (29)), we identify the filaments seen on the SEM images with the current-carrying branches of our discharge pattern.

6. Electrical Conduction along Chains of Ions: A Simple Model

We consider a linear chain of uniformly spaced Ag^+-ions with an interionic separation a, and a uniform conduction electron density to preserve overall charge neutrality inside the branches of the discharge pattern. In the one-dimensional conductor gaps appear at an electron wave number $k = \pm\pi/a$ in the one-dimensional single-electron energy band. Since there is one free electron per Ag^+-ion, the one-dimensional Fermi wave number is $k_F = \pm\pi/2a$, i.e., the Fermi energy is at the middle of the energy band.

Consider a linear chain of ions inside a given branch together with the associated electrons. Assume that an external DC electric voltage V_0 is applied across the branch. Considering that the total voltage V_0 applied across the branch is nearly equal to the voltage across the double layer near the cathode as in Figure 2 (to which case we restrict ourselves in the following), the electric field inside the double layer does the work eV_0 on the electron (e is the electronic charge). Based on the concepts developed to describe electrical conduction by CDWs [1, 7], we assume that the work eV_0 is transformed into the excitation energy of a collective mode, i.e. a longitudinal coupled ionic and electronic density wave of (angular) frequency

$$\omega = eV_0/\hbar \tag{7}$$

($\hbar$-Planck's constant h divided by 2π), travelling along a chain of Ag^+-ions inside a given branch. If the wavelength λ of the combined wave is twice the interionic separation a, i.e., if

$$\lambda = 2a \tag{8}$$

(or if the wave number of the combined wave is $q = 2\pi/\lambda = \pi/a = 2k_F$), then, due to the new periodicity introduced by the combined wave of wave number $q = 2k_F$, an energy gap, centred on the Fermi energy, occurs in the energy spectrum of single-electron states. This renders the new state energetically favourable because the electron kinetic energy of the occupied states being lowered to form the gap outweighs the elastic energy required to create the ionic distortion.

The propagation of the combined wave proceeds such that the ions oscillate with the frequency ω about their equilibrium positions, giving rise to an ionic density wave which propagates with the velocity of sound

$$v_s = \omega\lambda/2\pi, \tag{9}$$

whereas the electrons, participating in the electronic 'charge density wave' (CDW), are bodily displaced as a rigid entity with a drift velocity

$$v_d = (2eV_0/m^*)^{1/2} \tag{10}$$

equal to the velocity of sound v_s, i.e.,

$$v_d = v_s, \tag{11}$$

in this way carrying a current. (m^* is the effective mass of electrons in the CDW; see Section 9.)

The interionic separation a corresponds to a linear density of ions along a chain inside a given branch of

$$n = 1/a. \tag{12}$$

Since there is one conduction electron per Ag^+-ion, the linear electronic density is equal to n. Hence, when the electrons participating in the CDW move as a whole with the velocity v_d, the current per chain becomes

$$I_{chain} = env_d. \tag{13}$$

Combining (7) – (9) and (11), we obtain

$$v_d = eV_0a/\pi\hbar. \tag{14}$$

Equation (10) and (14) give

$$m^*v_da = h, \tag{15}$$

which says that the momentum m^*v_d successively proceeds step by step of a length equal to the interionic separation a, where m^*v_d is the momentum for which the action m^*v_da acquires its minimum, equal

to Planck's constant. For comparison, if the electron is displaced by jerks not only in one direction, but moves to and fro between two places at which it is reflected elastically (square well potential), then, according to the Bohr–Sommerfeld quantization rule, the phase integral extended over one motion to and fro becomes $2|m^* v_\mathrm{d}|a = nh$ ($n = 1,2,3,\ldots$), where a is the distance between the inversion points [8]. (A model for the motion of the CDW as represented by the jerky motion of a particle rolling down in a washboard potential which is tilted by the DC electric field has been proposed in [9].)

In principle, the CDW slides along the linear ionic lattice of Ag^+-ions inside a branch unattenuated with the velocity v_d. In real systems, however, pinning mechanisms will suppress the motion of the CDW [1]. In order to overcome pinning, application of an electric field $E = V_\mathrm{h}/l$ (depinning field) is required. The voltage V_h adjusts itself such that the electrons may continue to travel with the velocity v_d which they have gained across the double layer according to (14) and in this manner fulfil the conservation of the momentum $m^* v_\mathrm{d}$ according to (15). Elementary kinetic theory then leads to the formula

$$v_\mathrm{d}/E = e\tau/m^* \tag{16}$$

for the mobility furnished by the electrons, with τ the collective mode lifetime. Equations (15) and (16) give

$$eEa\tau = h, \tag{17}$$

which expresses that the energy eEa is taken up during time intervals τ, where eEa is the energy for which the action $eEa\tau$ has a minimum, equal to Planck's constant.

7. Conductivity

The DC conductivity of the high-conducting current path inside the bulk (in the following for short named 'high-conducting current path'),

$$\sigma_\mathrm{h} = l/R_\mathrm{h} wt, \tag{18}$$

on average, becomes, using (4)–(6),

$$\sigma_\mathrm{h} \cong 1.7 \cdot 10^{10}\ \Omega^{-1}\,\mathrm{cm}^{-1} = \text{const.}, \tag{19}$$
$$(l = 3\,\mathrm{cm},\ \ wt = 6 \cdot 10^{-4}\,\mathrm{cm}^2,\ \ R_\mathrm{h} = 3 \cdot 10^{-7}\,\Omega)$$

which conductivity is by a factor of $3 \cdot 10^4$ higher than the conductivity of metallic silver. The high-conducting current path obeys a linear $I - V_\mathrm{h}$ characteristic up to currents of 3–5 A only, the conductivity thereupon decreasing with increasing voltage V_h (and increasing total voltage V_0, respectively).

The conductivity (18) can be rewritten as

$$\sigma_\mathrm{h} = e n^{(3\mathrm{d})} v_\mathrm{d}/E, \tag{20}$$

where v_d (see (14)) is the drift velocity with which the electrons participating in the CDW are bodily displaced under the electric field

$$E = V_\mathrm{h}/l. \tag{21}$$

$n^{(3\mathrm{d})}$ is the three-dimensional electronic density inside a branch, or inside a current path if the branches are closely packed, given by

$$n^{(3\mathrm{d})} = (1/a)(1/b^2), \tag{22}$$

where $n = 1/a$ (see (12)) is the linear electronic density along a chain inside a branch; $1/b^2$ is the electronic density in a plane perpendicular to the chain direction with b^2 the cross-sectional area of a branch if one assumes the branches to be closely packed, which supposition seems to be confirmed by the SEM images in Figures 6b and 6d. With the current per chain $I_\mathrm{chain} = e n v_\mathrm{d}$ (see (13)) and the number N of chains connected in parallel, carrying the current

$$I = N I_\mathrm{chain} \tag{23}$$

through a current path of a cross-sectional area of

$$Nb^2 = wt, \tag{24}$$

we obtain (18), substituting (5), (12)–(14), and (21)–(24) into (20).

8. Quantities Characterizing the High-Conducting State

The current per chain (13) becomes, using (12) and (14),

$$I_\mathrm{chain} = 7.8 \cdot 10^{-5} V_0, \tag{25}$$

where I_chain is in Ampère and V_0 in Volt. This with a current of $I = 1$ A gives, using (1),

$$I_\mathrm{chain} \cong 1.1 \cdot 10^{-5}\ \mathrm{A}. \tag{26}$$

Using (1) and (25), the number of chains carrying the current I amounts to

$$N = I/I_{\text{chain}} \cong 9.2 \cdot 10^4 = \text{const.}, \tag{27}$$

independent of the value of I, since $V_0 \sim I$. Thus one branch occupies a cross-sectional area of, using (6) and (27),

$$b^2 = wt/N \cong 6.5 \cdot 10^{-9}\ \text{cm}^2 = \text{const.} \tag{28}$$

corresponding to a diameter of the branches of

$$b \cong 0.8 \cdot 10^{-4}\ \text{cm} = \text{const.} \tag{29}$$

By taking the interionic separation along a chain to be

$$a \cong 2.5 \cdot 10^{-8}\ \text{cm}, \tag{30}$$

about twice the ionic radius of a cation Ag^{1+} of $1.26 \cdot 10^{-8}$ cm, the 3d electronic density (22) becomes, using (28) and (30),

$$n^{(3\text{d})} \cong 6.1 \cdot 10^{15}\ \text{cm}^{-3} = \text{const.} \tag{31}$$

For the drift velocity (14), we obtain with a current of I = 1 A, using (1) and (30),

$$v_{\text{d}} \cong 1.7 \cdot 10^6\ \text{cm s}^{-1}. \tag{32}$$

The electric field (21) becomes with a current of I = 1 A, using (3) and (4),

$$E \cong 1.0 \cdot 10^{-7}\ \text{V cm}^{-1}. \tag{33}$$

Therefore the mobility is

$$v_{\text{d}}/E \cong 1.7 \cdot 10^{13}\ \text{cm}^2\ \text{V}^{-1}\ \text{s}^{-1} = \text{const.},$$

independent of the value of I, since $v_{\text{d}} \sim V_0 \sim I$ and $E \sim V_{\text{h}} \sim I$. The conductivity $\sigma_{\text{h}} \sim n^{(3\text{d})} v_{\text{d}}/E = \text{const.}$ (see (20)) likewise is independent of the value of I, as one must require for a matter constant.

For the current density per chain, we obtain from (2), (25), and (28)

$$I_{\text{chain}}/b^2 \cong 1.7 \cdot 10^3 I\,\text{cm}^{-2},$$

where I is in Ampère. Considering that the maximum current, which a current path can carry before the resistance R_{h} increases, is 3 – 5 A, the maximum current density which a chain can withstand turns out to be

$$I_{\text{chain}}/b^2 \cong 5.1 - 8.5 \cdot 10^3\ \text{A cm}^{-2}.$$

Larger currents must be taken over by the adjacent low-conducting matrix, which leads to the development of too much Joule heat and hence to the destruction of the high-conducting state. The temperature dependence of the critical current is difficult to obtain because the break in the slope of the $I - V_{\text{h}}$ characteristic, occurring where the destruction of the high-conducting state takes place, is not very sharp.

The minimum distance between neighbouring chains inside the branches is equal to the diameter $b \cong 10^{-4}$ cm of the branches, reached when the branches are closely packed. This large distance suggests that pinning of the CDWs due to Coulomb interaction between CDWs on neighbouring chains, which causes transverse correlation effects, can be neglected. Pinning provided by the commensurability [10] between the CDW wavelength and the lattice (when, as in (8), the CDW wavelength λ is an integral multiple of the lattice spacing a) can be overcome by the thermal generation of dislocations or discommensurations [11], which allow the CDWs to slide along the chains without climbing a potential barrier. CDWs, which have become pinned to the underlying linear lattice by lattice imperfections and impurities, will be, to our knowledge, depinned by weak electric fields, as discussed in Section 6.

9. Effective Mass of Electrons and Collective Mode Lifetime

From (15), we can associate an effective mass with the electrons participating in the CDW given by

$$m^* = h/(v_{\text{d}} a), \tag{34}$$

which becomes with a current of I = 1 A, using (30) and (32),

$$m^* \cong 1.7 \cdot 10^2\ \text{m} \tag{35}$$

(m is the free-electron mass), increasing with decreasing $v_{\text{d}} \sim V_0 \sim I$. The effective masses have been obtained from low frequency AC conductivity and static dielectric constant measurements utilizing the oscillations of the pinned CDW about its equilibrium position. Their magnitudes in the organic charge transfer salt tetrathiafulvalene-tetracyanoquinodimethane (TTF-TCNQ) and the organometallic compound potassium platinocyanide (KCP), which show evidence of electron transport via moving CDWs, are ≅ 300 m and

$\cong 10^3$ m, respectively [12]. A comparison with our result, however, becomes questionable because the experiments have been analyzed in terms of an equation of motion, describing the dynamics of the pinned CDW, which does not take into account that the effective mass may be current-dependent.

Equation (34) can be rewritten, considering that the instant at which an electron passes a given ion in the chain is not determined precisely, but carries an uncertainty

$$\Delta t \cong a/v_\mathrm{d}, \tag{36}$$

leading from the uncertainty principle to a spread of the energy of an electron of

$$\Delta E \cong h/\Delta t. \tag{37}$$

Equations (36) and (37) inserted into (34) give

$$m^* \cong h^2/(a^2 \Delta E). \tag{38}$$

With $v_\mathrm{d} \sim V_0 \sim I \to 0$, $m^* \to \infty$, and $\Delta E \to 0$, i.e., the system in the classical macroscopic limit has a well-defined energy, the uncertainty ΔE in the energy of an electron becoming infinitely small.

Equation (38) is of the same form as the effective mass valid in the tightly bound electron approximation for normal-conducting electrons in a one-dimensional periodic potential with the period a [13]. As the binding energy of the electrons increases (corresponding to a decreasing band width ΔE), the effective mass of the electrons increases. The electrons in the CDW will be stronger bound and, hence, will have a larger effective mass than free electrons, because the electrons will have lower energy in regions where the ions in the chain are more closely spaced and the electrons, therefore, tend to concentrate in the regions of greater positive charge to form the CDW.

The collective mode lifetime becomes with a current of $I = 1$ A, using (17), (30), and (33),

$$\tau \cong 1.6\,\mathrm{s}, \tag{39}$$

increasing with decreasing $E \sim V_\mathrm{h} \sim I$, which is plausible since with simultaneously increasing mass m^* the CDW will be increasingly less scattered. We have detected circulating currents induced in ring-shaped samples by switching off an external magnetic field which first permeates the hole of the ring-shaped sample [14]. Currents, induced in the ring, can circulate over a period of the order of the collective mode lifetime τ of relation (39). The strength of the circulating current then must have been of the order of 1 A.

10. Transient Current

In Figure 7 a DC voltage of 5 V is applied to the current electrodes, with the circuit first open, the cathode connected to earth and the high-conducting current path. When thereupon the anode is put down to the current path, a transient current I of $1-1.5$ μA flows for about 1 s from the earth to the anode along the high-conducting current path, while the parallel-connected circuit together with the current supply is short-circuited by the high-conducting current path. The current driven by the current supply along the circuit (limited to 1 A) will not be detected by the μA-meter. (The current flows in the opposite direction if the polarity in the circuit diagram in Figure 7 is reversed with the anode now connected to earth.) If instead of the high-conducting current path a strand, sheet or bar of copper is inserted, no transient current is observed.

If the anode (or cathode) is put down, an electric field arises throughout all the conductors of the network. As a consequence, a transient current must flow which tends to produce a charge distribution which just compensates the external field. However, in the normal conductors the electrostatic equilibrium will be reestablished in a time too short to become observable. In the high-conducting current path this time will be long: it is the long-range phase coherence in the collective CDW mode [1] which hinders the electrons from effectively acting as equalizing charges.

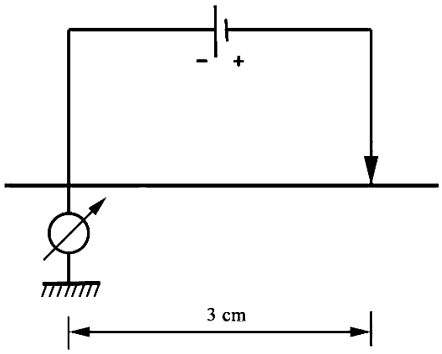

Fig. 7. Circuit diagram used for the detection of transient currents.

The electron charge contained in the high-conducting current path is

$$Q = en^{(3d)}wtl \cong 1.8 \cdot 10^{-6}\,\mathrm{A\,s},$$

where $n^{(3d)} \cong 6.1 \cdot 10^{15}\,\mathrm{cm}^{-3}$ (see (31)) is the electronic density inside the current path, $wt \cong 6.0 \cdot 10^{-4}\,\mathrm{cm}^2$ (see (6)) the cross-sectional area of the current path, and $l = 3\,\mathrm{cm}$ its length. Then the transient current, i.e. the ratio of the charge Q to the period of about 1 s, during which this charge crosses a given cross section of the current path, becomes

$$I = en^{(3d)}wtl/1\,\mathrm{s} \cong 1.8\,\mu\mathrm{A},$$

which current, in order to guarantee the continuity of current, also must flow through the earth wire, where it becomes observable. The electron charge (current strength × duration of current flow) remains approximately the same, when one varies the applied voltage, the current strength increasing and the duration of current flow decreasing, respectively, with increasing voltage. The correct transient current obtained provides a direct test for the density $n^{(3d)}$ calculated from (22).

Additional evidence for that the conduction mechanism is non-trivial is given by the finding that the resistance along a number N of branches connected in parallel increases in quantized steps of height $h/2e^2N$ with increasing voltage applied across the branches [7].

11. Concluding Remark: Radius of Branches Determined during the Passage of the Spark

The radius $b/2$ of the branches is presumably determined by the radial ambipolar diffusional expansion of the plasma of ions and electrons inside the branches during the passage of the spark, opposed to the tendency of ions and electrons to form linear chains along the axis of the branches.

A branch expands owing to the radial movement of the plasma as long as the spark, propagating with the velocity

$$v^{\mathrm{spark}} \cong 3\,\mathrm{cm}/3\,\mathrm{s}$$

(see Section 2), passes a given ion across the interionic separation a, which takes a time $t_a \cong a/v^{\mathrm{spark}}$, during which a given ion acts upon one and the same electron and, hence, ion and electron diffuse both together. The radius of the branch reached during that time is given by the diffusion law

$$b/2 = (D_{\mathrm{a}}t_a)^{1/2},$$

where D_{a} is the diffusion coefficient for ambipolar diffusion. On taking $D_{\mathrm{a}} \cong 2\,\mathrm{cm}^2/\mathrm{s}$ [5, p. 359], valid for the plasma of a spark channel of comparable ionic and electronic density ($10^{14} - 10^{16}\,\mathrm{cm}^{-3}$) in gas discharges, we obtain, using (30),

$$b/2 \cong 2 \cdot 10^{-4}\,\mathrm{cm},$$

which agrees, to order of magnitude, with the experimental value in Section 5.

Acknowledgement

The author gratefully acknowledges the help of M. Eiswirth and S. Wasle (Fritz-Haber-Institut der Max-Planck-Gesellschaft, Berlin) for assistance and reproduction of the measurements. Special thanks to G. Weinberg (FHI) who carried out the electron microscopy studies.

[1] G. Grüner, Rev. Mod. Phys. **60**, 1129 (1988).
[2] I. Prigogine, G. Nicolis, and A. Babloyantz, Phys. Today, November (1972), pp. 23 – 28.
[3] P. Arendt, Eur. Phys. J. Appl. Phys. **30**, 41 (2005).
[4] J. K. Kjems, in: Fractals and Disordered Systems (Eds. A. Bunde, S. Havlin), Springer, Berlin 1991, p. 303.
[5] Y. P. Raizer, Gas Discharge Physics, Springer, Berlin 1991.
[6] J. O'M. Bockris, N. Bonciocat, and F. Gutmann, An Introduction to Electrochemical Science, Wykeham Publications, London 1974, Chap. 3.
[7] P. Arendt, Eur. Phys. J. Appl. Phys. **36**, 149 (2006).
[8] F. Hund, Einführung in die Theoretische Physik, Bibliograph. Inst., Leipzig 1950, Bd. 5, pp. 101 – 103.
[9] G. Grüner, Comments Solid State Phys. **10**, 183 (1983).
[10] P. A. Lee, T. M. Rice, and P. W. Anderson, Solid State Commun. **14**, 703 (1974).
[11] N. P. Ong, Can. J. Phys. **60**, 757 (1982).
[12] M. J. Rice, Physics Bulletin, November (1975), pp. 493 – 495.
[13] K. Kreher, Festkörperphysik, Akademie-Verlag, Berlin 1973, pp. 102 – 111.
[14] P. Arendt, to be published.